

TORSIONAL RIGIDITIES OF CANCELLOUS BONE FILLED WITH MARROW: THE APPLICATION OF MULTIPOINT PADÉ APPROXIMANTS

S. T O K A R Z E W S K I, J. J. T E L E G A, A. G A Ł K A

**INSTITUTE OF FUNDAMENTAL TECHNOLOGICAL RESEARCH
POLISH ACADEMY OF SCIENCES**

Świętokrzyska 21, 00-049 Warsaw, Poland

e-mail: stokarz@ippt.gov.pl; jtelega@ippt.gov.pl; agalka@ippt.gov.pl

An idealized model of prism-like trabecular bone was developed to study its static and dynamic responses under torsional moments. Effects of bone marrow and bone apparent density were investigated. By constructing multipoint Padé approximants [1, 2] to the torsional complex modulus, hydraulic stiffening of the prism-like bone due to the presence of bone marrow was predicted. The torsional compliance, creep function and relaxation function were also evaluated.

1. INTRODUCTION

Trabecular bone is a porous structure consisting of bony network of connecting rods, plates and prisms (elastic phase) filled with bone marrow (viscous phase). Various approaches to modelling the mechanical behaviour of trabecular bone as a continuum have been proposed, see [10, 13, 15] and [35]. By assuming the trabecular bone to be a solid, only apparent material properties can be obtained, and this assumption is not valid over the length scales close to microstructural dimensions, cf. [14]. In order to study the states of stress and strain in individual trabeculae, microstructural analysis is required. This is important in bone biomechanical processes, such as bone remodelling, and in mechanical processes, such as trabecular bone fatigue, which are most likely affected by trabecular tissue stresses and strains [17].

Microstructure analysis of trabecular bone has followed the general approach used in modelling cellular plastics. MCELHANEY *et al.* [18] developed a porous block model of trabecular bone based on integration of spring stiffness, loaded in parallel or in series. Using this model, these authors found good agreement between prediction of apparent stiffness and the experimentally measured stiffness values in some internal layer of human skull. PUGH *et al.* [24] modelled the subchondral trabecular bone as a collection of structural plates and concluded that bending and buckling were major modes of deformation of the trabeculae. WILLIAMS and LEWIS [35] modelled the exact structure of two-dimensional section of trabecular bone with plane strain finite elements to predict the apparent transversely isotropic elastic constants. GIBSON [10] developed models of trabecular bone structure using analytical techniques for porous solids. He predicted the dependence of apparent stiffness on apparent density for different structural types of trabecular bones. BEAUPRÉ and HAYES [3] developed a three-dimensional spherical void model of trabecular bone and used finite element analyses to predict apparent stiffness and strength, as well the stress distribution within the trabeculae. HOLLISTER *et al.* [15] applied the homogenization theory [25] for an investigation of mechanical behaviour of cubic rod-like structures modelling trabecular bones. By using finite element method these authors evaluated the apparent, orthogonal Young's moduli and compared them with the experimental data obtained for proximal humerus, proximal tibia and distal femur. In the structural models discussed above only the static response of the trabecular structure has been studied and the effect of bone marrow has not been considered.

Hydraulic stiffening of trabecular bone due to the presence of bone marrow has been exhibited in the the papers [5] and [21]. More precisely, CARTER and HAYES [5] performed compression tests on trabecular bone samples at different strain rates. These authors claim that at elevated strain rates the viscosity effect of bone marrow in increasing bone strength and stiffness become significant. OCHOA *et al.* [21] measured femoral head stiffness and studied its changes by altering the fluid boundary condition. They suggested that a mechanical strengthening mechanism due to fluid may be present in intact trabecular bone, and the overall stiffness reflects the material properties of both the porous solid matrix and the entrapped fluid. KASRA and GRYNPAS [16] analyzed the idealized structural model of vertebral trabecular bone under compressive loading. These authors also predicted hydraulic stiffening of trabecular bone due to the presence of bone marrow.

Both the compact and trabecular bones exhibit time-dependent behavior, however at rather elevated strain rates. The paper by TELEGA and LEKSZYCKI [29] provides, among others, a review of inelastic and torsional behavior of bone.

The reader is referred to this comprehensive paper for relevant references. The excellent book by TAVASSOLI and YOFFEY [26] offers a systematic study of structure and function of bone marrow. However, its mechanical properties have not been included. Therefore we treat marrow as a viscous material and present the results of calculation in a nondimensional form.

More precisely, an idealized structural model of a prismatic cancellous bone filled with bone marrow has been developed in order to study its static and dynamic response under torsional loadings. Our main goal is to derive analytical formulae relating effective torsional moduli such as complex modulus, complex compliance, creep and relaxation functions to the apparent density of the trabecular bone and viscosity of a bone marrow. To this end, the homogenization procedure [25] and multipoint Padé approximants ([2, 30, 31, 32]) have been successfully applied.

2. MATHEMATICAL MODEL OF A PRISM-LIKE CANCELLOUS BONE

Let us consider a two-phase material consisting of elastic porous solid filled with viscoelastic fluid. Such an idealized composite material is used to model a trabecular bone. Assume that $\lambda_1^* = \lambda_1' + i\lambda_1''$ and $\mu_1^* = \mu_1' + i\mu_1''$ are complex moduli of the solid phase, while $\lambda_2^* = \lambda_2' + i\lambda_2''$ and $\mu_2^* = \mu_2' + i\mu_2''$ characterize the viscoelastic properties of the fluid phase. Note that the case $\lambda_1' = 0, \mu_1' = 0$ and $\lambda_2' = 0, \mu_2' = 0$ represents a material consisting of a porous elastic matrix filled with a Newtonian fluid.

For the oscillating viscoelastic solid-fluid composite the governing equations take the form

$$(2.1) \quad \sigma_{ij,j}^n = 0 \quad \text{on } \Omega, \quad n = 0, 1,$$

where

$$(2.2) \quad \sigma_{ij}^n = \lambda_n^* u_{k,k}^n \delta_{ij} + \mu_n^* (u_{i,j}^n + u_{j,i}^n) \quad \text{in } \Omega, \quad n = 1, 2.$$

The interface conditions are given by

$$(2.3) \quad u_i^1 = u_i^2, \quad \sigma_{ij}^1 m_j = \sigma_{ij}^2 m_j \quad \text{on } \partial\Omega.$$

The boundary condition is classical

$$(2.4) \quad \sigma_{ij}^1 m_j = g_i \quad \text{on } \partial\Omega.$$

Here $\sigma_{ij}^1, \sigma_{ij}^2, u_i^1$ and u_i^2 denote the components of stress and displacement fields in the solid and fluid phases respectively, while g_i are prescribed. The geometry

of the composite material is defined by: $\overset{1}{\Omega}$ is the domain occupied by a matrix, while $\overset{2}{\Omega}$ denotes the domain occupied by fluid, $\Omega = \overset{1}{\Omega} \cup \overset{2}{\Omega}$ is the domain occupied by the composite material, $\overset{1}{\partial\Omega}$ and $\overset{2}{\partial\Omega}$ are the surfaces enclosing the solid and fluid phases, respectively. As usual $\partial\Omega$ denotes the boundary of Ω , \mathbf{m} stands for the unit vector normal to $\overset{1}{\partial\Omega}$ and $\overset{2}{\partial\Omega}$ and is directed outwards.

3. TORSION OF AN INHOMOGENEOUS BEAM

Consider a porous beam filled with a fluid. Assume that at the opposite ends of the beam the torsional moments are applied. For such a case the displacement field takes the form [19]

$$(3.1) \quad u_1 = -\alpha x_3 x_2, \quad u_2 = \alpha x_3 x_1, \quad u_3 = \alpha \beta(x_1, x_2) \quad \text{in } \Omega = \overset{1}{\Omega} \cup \overset{2}{\Omega},$$

$$(3.2) \quad \sigma_{11} = \sigma_{22} = \sigma_{33} = \sigma_{12} = \sigma_{21} = 0 \quad \text{in } \Omega = \overset{1}{\Omega} \cup \overset{2}{\Omega}.$$

The parameter α denotes the torsional angle of unit length of the beam. By substituting (3.1) – (3.2) to (2.1) – (2.4) we obtain

$$(3.3) \quad \sigma_{k3} = \alpha \Gamma^*(x) \frac{\partial}{\partial x_k} \left((\beta(x) + (-1)^k x_k x_{k\pm 1}) \right) \quad \text{in } \Omega, \quad k = 1, 2;$$

$$x = (x_1, x_2),$$

where

$$(3.4) \quad x_{k\pm 1} = \begin{cases} x_{k+1}, & \text{if } k = 1, \\ x_{k-1}, & \text{if } k = 2. \end{cases}, \quad \Gamma^*(x) = \Theta_1(x)\mu_1^* + \Theta_2(x)\mu_2^*.$$

Here $\Theta_i(x)$, $i = 1, 2$, are the characteristic functions: $\Theta_i(x) = 1$ ($\Theta_i(x) = 0$), if x belongs (does not belong) to the phase i . The stresses σ_{k3} given by Eq. (3.3) satisfy the equilibrium equation, cf. [7],

$$(3.5) \quad \sum_{k=1}^2 \frac{\partial}{\partial x_k} \left[\Gamma^*(x) \frac{\partial}{\partial x_k} \left(\beta(x) + (-1)^k x_k x_{k\pm 1} \right) \right] = 0 \quad \text{in } \Omega,$$

and the interface condition

$$(3.6) \quad \sum_{k=1}^2 \Gamma^*(x) \frac{\partial}{\partial x_k} \left(\beta(x) + (-1)^k x_k x_{k\pm 1} \right) m_k = 0 \quad \text{on } \partial\Omega.$$

Here $\overset{l}{\partial\Omega}$ denotes the lateral surface of the beam, while $\Gamma^*(x)$ is the complex shear modulus. The set of Eqs. (3.1) – (3.2) and (3.5) – (3.6) describe the torsional

response of the prismatic solid-fluid beam under harmonically oscillating external moments.

4. HOMOGENIZATION OF AN ANISOTROPIC INHOMOGENEOUS BEAM

In the sequel we restrict our considerations to a periodic distribution of shear modulus now represented by

$$(4.1) \quad \Gamma^*(x) = \Gamma^{*\varepsilon}(x) = \Gamma^*\left(\frac{x}{\varepsilon}\right),$$

where $\varepsilon > 0$ is a small, nondimensional parameter characterizing the periodicity of a cross-sectional microstructure of the porous beam. By substituting (4.1) into (3.5) one obtains

$$(4.2) \quad \sum_{k=1}^2 \frac{\partial}{\partial x_k} \left[\Gamma^*\left(\frac{x}{\varepsilon}\right) \frac{\partial}{\partial x_k} \left(\beta^\varepsilon(x) + (-1)^k x_k x_{k\pm 1} \right) \right] = 0 \quad \text{in } \partial\Omega.$$

To solve Eq. (4.1), the method of two-scale asymptotic is applied. Thus we write, cf. [4, 5],

$$(4.3) \quad \beta^\varepsilon(x) = w_o(x, y) + \varepsilon w_1(x, y) + \varepsilon^2 w_2(x, y) + \dots, \quad y = x/\varepsilon, \quad y \in Y.$$

Here Y is the two-dimensional unit cell. We set

$$(4.4) \quad \begin{aligned} A_0^{(k)} &= \frac{\partial}{\partial y_k} \left(\Gamma^*(y) \frac{\partial}{\partial y_k} \right), \\ A_1^{(k)} &= \frac{\partial}{\partial y_k} \left(\Gamma^*(y) \frac{\partial}{\partial x_k} \right) + \Gamma^*(y) \frac{\partial}{\partial x_k} \frac{\partial}{\partial y_k}, \\ A_2^{(k)} &= \Gamma^*(y) \frac{\partial}{\partial x_k} \frac{\partial}{\partial x_k}. \end{aligned}$$

We recall that Γ^* is now a complex function. Formally, the method of asymptotic expansions proceeds similarly to the case of real coefficients. Then Eq. (4.2) takes the following form:

$$(4.5) \quad \sum_{k=1}^2 \left(\varepsilon^{-2} A_0^{(k)} + \varepsilon^{-1} A_1^{(k)} + A_2^{(k)} \right) \left(w_o + (-1)^k x_k x_{k\pm 1} + \varepsilon w_1 + \dots \right) = 0.$$

Comparing the terms containing equal powers of ε we get

$$(4.6) \quad \begin{aligned} & \sum_{k=1}^2 A_0^{(k)} (w_0 + (-1)^k x_k x_{k\pm 1}) = 0, \\ & \sum_{j=1}^2 A_0^{(j)} w_1 + \sum_{k=1}^2 A_1^{(k)} (w_0 + (-1)^k x_k x_{k\pm 1}) = 0, \\ & \sum_{j=1}^2 (A_0^{(j)} w_2 + A_1^{(j)} w_1) + \sum_{k=1}^2 A_2^{(k)} (w_0 + (-1)^k x_k x_{k\pm 1}) = 0. \end{aligned}$$

The standard procedure shows that, cf. [4, 5],

$$(4.7) \quad w_0(x, y) = f(x),$$

and

$$(4.8) \quad w_1(x, y) = - \sum_{k=1}^2 \chi^k(y) \frac{\partial}{\partial x_k} (f(x) + (-1)^j x_k x_{k\pm 1}) + f_1(x),$$

where $f_1(x)$ is an arbitrary function of x , while $\chi^k(y)$, $k = 1, 2$ is a solution to

$$(4.9) \quad \sum_{j=1}^2 A_0^{(j)} \chi^k(y) = \frac{\partial}{\partial y_k} \Gamma^*(y), \quad \chi^k(y) \text{ } Y\text{-periodic.}$$

Equation (4.9) has a Y -periodic solution, provided that

$$(4.10) \quad \int_Y \left(\sum_{j=1}^2 A_1^{(j)} w_1 + \sum_{k=1}^2 A_2^{(k)} (w_0 + (-1)^k x_k x_{k\pm 1}) \right) dy = 0.$$

Substituting (4.7) and (4.8) into (4.10) we obtain

$$(4.11) \quad \begin{aligned} & - \int_Y \sum_{j=1}^2 \sum_{k=1}^2 \frac{\partial}{\partial y_j} (\Gamma^*(y) \chi^k(y)) \frac{\partial^2}{\partial x_j \partial x_k} (f(x) + (-1)^j x_k x_{k\pm 1}) dy \\ & + \int_Y \sum_{j=1}^2 \frac{\partial \Gamma^*(y)}{\partial y_j} \frac{\partial f_1(x)}{\partial x_j} dy + \int_Y \sum_{j=1}^2 \sum_{k=1}^2 \Gamma^*(y) \left(\delta_{jk} - \frac{\partial \chi^k(y)}{\partial y_j} \right) \\ & \cdot \frac{\partial^2}{\partial x_j \partial x_k} (f(x) + (-1)^j x_k x_{k\pm 1}) dy = 0. \end{aligned}$$

Since the functions $\Gamma^*(y)$ and $\chi^k(y)$ are Y -periodic, the first two integrals appearing in (4.11) vanish. Thus we arrive at the following homogenized bound-

ary value problem: find the function f such that

$$(4.12) \quad \begin{aligned} \sum_{j=1}^2 \sum_{k=1}^2 Q_{jk}^* \frac{\partial^2}{\partial x_j \partial x_k} \left(f(x) + (-1)^j x_k x_{k\pm 1} \right) &= 0, \\ \sum_{k=1}^2 Q_{jk}^* \frac{\partial}{\partial x_k} \left(f(x) + (-1)^k x_k x_{k\pm 1} \right) m_k &= 0. \end{aligned}$$

Here

$$(4.13) \quad Q_{jk}^* = \int_Y \Gamma^*(y) \left(\delta_{jk} - \frac{\partial \chi^k(y)}{\partial y_j} \right) dy,$$

are the *homogenized* coefficients. We recall the Y - periodic functions χ^k are solution to Eq. (49). By substituting $\chi^k(y) = y_k - T^k(y)$ into (4.9) and (4.13) we obtain

$$(4.14) \quad Q_{jk}^* = \int_Y \Gamma^*(y) \frac{\partial T^k(y)}{\partial y_j} dy, \quad j, k = 1, 2,$$

where $T^k(y)$ are determined by

$$(4.15) \quad \sum_{j=1}^2 \frac{\partial}{\partial y_j} \left(\Gamma^*(y) \frac{\partial T^k(y)}{\partial y_j} \right) = 0, \quad (y_k - T^k(y)) \text{ is } Y - \text{ periodic.}$$

Relations (4.14) – (4.15), where $\Gamma^*(y)$ is given by (3.4), were investigated in [12] in the context of dielectric coefficients of two-phase composite materials. Due to the results obtained in [12], the effective torsional moduli $Q_{jk}^*(z)/\mu_1$ have a Stieltjes integral representation of the form

$$(4.16) \quad \frac{Q_{jk}^*(z)}{\mu_1} - 1 = z \int_0^1 \frac{d\beta_{jk}(v)}{1 + zv}, \quad z = \frac{\mu_2^*}{\mu_1^*} - 1,$$

where the matrix $[\beta_{jk}(v)]$ is positive definite, while $\beta_{11}(v)$, $\beta_{22}(v)$ are non-decreasing functions.

5. HOMOGENIZATION OF INHOMOGENEOUS BEAM WITH ISOTROPIC SYMMETRY

Let us consider an inhomogeneous beam consisting of cylinders filled with a fluid, regularly spaced in a solid phase. Such an idealized system models prismatic cancellous bone filled with marrow, see Fig. 1. For the prismatic beam shown in Fig. 1b we have $T^1 = T^2 = T$, $Q_{11}^* = Q_{22}^* = Q^*$ and $Q_{12}^* = Q_{21}^* = 0$. On

account of that, the anisotropic boundary value problem (4.14) – (4.15) reduces to the isotropic one:

$$(5.1) \quad Q^* = \int_Y \Gamma^*(y) \frac{\partial T(y)}{\partial y_1} dy,$$

where

$$(5.2) \quad \frac{\partial}{\partial y_1} \left(\Gamma^*(y) \frac{\partial T(y)}{\partial y_1} \right) + \frac{\partial}{\partial y_2} \left(\Gamma^*(y) \frac{\partial T(y)}{\partial y_2} \right) = 0,$$

($y_1 - T(y)$) is Y – periodic

REMARK 1.

We observe that replacing in Eqs. (5.1) and (5.2) the complex modulus $\Gamma^*(y)$ by the corresponding real modulus $\Gamma(y)$ one obtains the equations defining the effective shear modulus Q for a beam with elastic phases. Conversely, the replacement of $\Gamma(y)$ by $\Gamma^*(y)$ transforms the real effective modulus Q to the corresponding complex one Q^* .

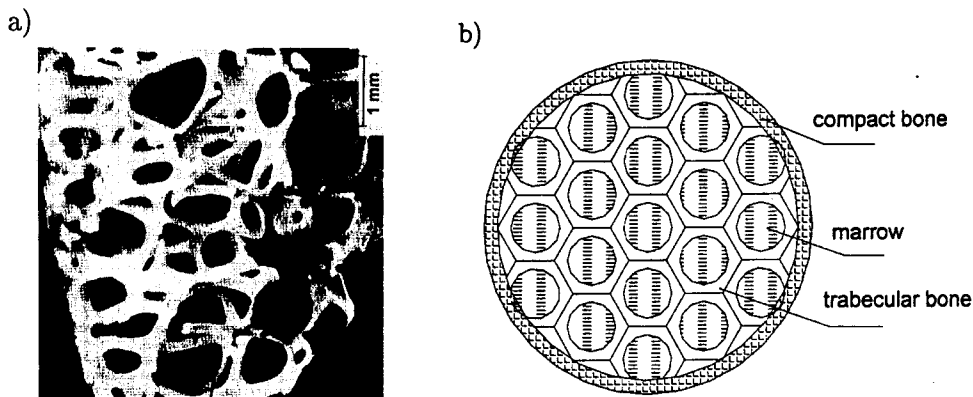


FIG. 1. (a) The scanning electron micrograph showing a prismatic structure of cancellous bone; a sample taken from the femoral head, after [11], pp. 318. (b) An idealized structural model of a prism-like cancellous bone.

In the next section Eqs. (5.1), (5.2) will be solved for a composite material consisting of elastic cylinders embedded in an elastic matrix.

6. HEXAGONAL ARRAY OF ELASTIC CYLINDERS

Let us study a hexagonal array of elastic cylinders embedded in an elastic matrix. For such a case the parameters μ_1^* , μ_2^* and consequently $z = \mu_2^*/\mu_1^* - 1$

take real values only. For convenience we set $Q^* = Q$, $\mu_1^* = \mu_1' = \mu_1$, $\mu_2^* = \mu_2' = \mu_2$ and $z = X$. From (4.16), it follows that the solution $Q(X)/\mu_1$ of the boundary value problem (5.1), (5.2) has a Stieltjes integral representation

$$(6.1) \quad \frac{Q(X)}{\mu_1} - 1 = z \int_0^1 \frac{d\beta(v)}{1 + Xv}, \quad X = \frac{\mu_2}{\mu_1} - 1,$$

where $\beta(v) = \beta_{11}(v) = \beta_{22}(v)$. In order to find $Q(X)/\mu_1$ defined by Eqs. (5.1) - (5.2), the multipoint Padé technique will be applied, cf. [30]. That technique requires the following input data:

(i) The discrete values of $(Q(\varphi, X)/\mu_1) - 1$ given at $\varphi = \varphi_j$ and $X = X_i$, see Table 1.

Table 1. Discrete values of the elastic torsional modulus $Q(X)/\mu_1 - 1$ for the hexagonal array of cylinders, after [23].

x	$\varphi=0.76$	$\varphi=0.80$	$\varphi=0.84$	$\varphi=0.88$
-1	-0.8711	-0.8996	-0.9286	-0.9607
0	0.0000	0.0000	0.0000	0.0000
9	3.3778	3.9489	4.6887	5.7225
49	5.7076	7.2600	9.7931	5.1565
∞	6.7600	8.9586	3.0093	24.4508

(ii) The expansion of $(Q(X)/\mu_1) - 1$ at $X = 0$ given by $(Q(X)/\mu_1) - 1 = \varphi X + 0.5\varphi(1 - \varphi)X^2 + O(X^3)$.

In the present paper the following rational functions

$$(6.2) \quad [M/M](X) = \frac{a_{M1}X + a_{M2}X^2 + \dots + a_{MM}X^M}{1 + b_{M1}X + b_{M2}X^2 + \dots + b_{MM}X^M},$$

$$[M - 1/M - 1](X) = \frac{\check{a}_{(M-1)1}X + \check{a}_{(M-1)2}X^2 + \dots + \check{a}_{(M-1)M-1}X^{M-1}}{1 + \check{b}_{(M-1)1}X + \check{b}_{(M-1)2}X^2 + \dots + \check{b}_{(M-1)M-1}X^{M-1}},$$

define the multipoint Padé approximants $[M/M](X)$ and $[M - 1/M - 1](X)$ to $(Q(X)/\mu_1) - 1$ respectively, cf. [32]. The coefficients a_{Mk} , b_{Mk} ($k = 1, 2, \dots, M$) and $\check{a}_{(M-1)j}$, $\check{b}_{(M-1)j}$ ($j = 1, 2, \dots, M - 1$) are defined by $2M$ equations for $[M/M]$

$$(6.3) \quad [M/M](X) = \varphi X + 0.5X(1 - \varphi)X^2 + O(X^3),$$

$$[M/M](X_i) = (Q(X_i)/\mu_1) - 1, \quad \text{for } X_{-1}, \quad -1 < X_i < \infty,$$

$$i = 1, 2, \dots, 2M - 4,$$

and $2M - 2$ relations for $[M - 1/M - 1]$

$$(6.4) \quad [M - 1/M - 1](X) = \varphi X + 0.5X(1 - \varphi)X^2 + O(X^3),$$

$$[M - 1/M - 1](X_i) = (Q(X_i)/\mu_1) - 1 \quad \text{for } -1 < X_i < \infty, \\ i = 1, 2, \dots, 2M - 4.$$

In [30] it has been proved that $Q(X)/\mu_1$ satisfies the following inequalities

$$(6.5) \quad (-1)^{K_L} [M/M](X) \leq (-1)^{K_L} [Q(X)/\mu_1 - 1] \leq (-1)^{K_L} [M - 1/M - 1](X).$$

Here K_L denotes the number of the input data given at points X_i belonging to the interval $[-1, X)$. By starting from the values $[(Q(\varphi_i, X_i)/\mu_1) - 1]$ depicted in Table 1 and the coefficients φ and $0.5\varphi(1 - \varphi)$ of power expansion of $[(Q(X)/\mu_1) - 1]$, the multipoint Padé approximants $1 + [3/3](X)$ and $1 + [2/2](X)$ are evaluated and gathered in Table 2. Those approximants estimate of $Q(X)/\mu_1$ is as follows:

$$(6.6) \quad (-1)^{K_L} (1 + [3/3](X)) \leq (-1)^{K_L} Q(X)/\mu_1 \leq (-1)^{K_L} (1 + [2/2](X)).$$

Table 2. Multipoint Padé approximants $1 + [3/3]$ and $1 + [2/2]$ to torsional modulus $Q(X)/\mu_1$ of a hexagonal array of elastic cylinders embedded in an elastic beam; φ -volume fraction.

φ	$1 + [3/3](X)$	$1 + [2/2](X)$
0.76	$\frac{1 + 1.7328X + 0.9159X^2 + 0.1476X^3}{1 + 0.9728X + 0.2678X^2 + 0.0190X^3}$	$\frac{1 + 1.3460X + 0.4066X^2}{1 + 0.5860X + 0.0524X^2}$
0.80	$\frac{1 + 1.8655X + 1.0787X^2 + 0.1910X^3}{1 + 1.0655X + 0.3063X^2 + 0.0192X^3}$	$\frac{1 + 1.3364X + 0.3881X^2}{1 + 0.5364X + 0.0390X^2}$
0.84	$\frac{1 + 1.8901X + 1.0865X^2 + 0.1816X^3}{1 + 1.0501X + 0.2717X^2 + 0.0130X^3}$	$\frac{1 + 1.3048X + 0.3481X^2}{1 + 0.4648X + 0.0249X^2}$
0.88	$\frac{1 + 1.8582X + 1.0009X^2 + 0.1345X^3}{1 + 0.9782X + 0.1929X^2 + 0.0053X^3}$	$\frac{1 + 1.2331X + 0.2685X^2}{1 + 0.3531X + 0.0106X^2}$

Figure 2 depicts: a) the Padé bounds $1 + [3/3](X)$ and $1 + [2/2](X)$ on torsional modulus $Q(X)/\mu_1$, b) the approximation error $\xi = 100\% \times \{[3/3](X) - [2/2](X)\} / \{1 + [3/3](X)\}$, $X = \mu_2/\mu_1 - 1$ for $Q(X)/\mu_1$.

From Fig. 2 we conclude that the torsional modulus $Q(X)/\mu_1$ differs from the multipoint Padé approximants $1 + [3/3](X)$ and $1 + [2/2](X)$ by less than 0.3%. On account of that we assume that the function

$$(6.7) \quad Q(X)/\mu_1 = 1 + [3/3](X), \quad X = (\mu_2/\mu_1) - 1, \varphi \leq 0.88$$

provides a good estimate of the effective torsional modulus.

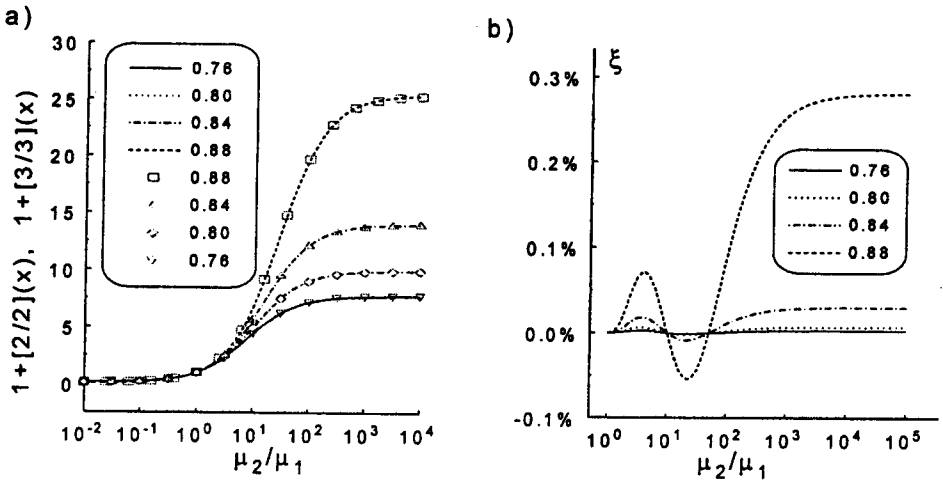


FIG. 2. Hexagonal array of elastic cylinders with volume fraction φ and physical parameter $X = (\mu_2/\mu_1) - 1$; (a) multipoint Padé bounds $1 + [3/3](X)$ (conventional lines) and $1 + [2/2](X)$ (scattered line) on the torsional modulus $Q(X)/\mu_1$; (b) error $\xi = 100\% \times \{[3/3](X) - [2/2](X)\} / \{1 + [3/3](X)\}$ for $Q(X)/\mu_1$.

7. HEXAGONAL ARRAY OF FLUID CYLINDERS

Consider now a hexagonal array of cylinders filled with viscous fluid embedded in an elastic beam. For such a case the parameters μ_1^* , μ_2^* and consequently $z = \mu_2^*/\mu_1^* - 1$ take complex values. On account of Remark 5, by replacing X in (6.7) by z one obtains the complex torsional modulus $Q^*(z)/\mu_1$:

$$(7.1) \quad Q^*(z)/\mu_1 = 1 + [3/3](z) \text{ for } \varphi \leq 0.88, z = I\omega\mu_2/\mu_1 - 1.$$

Here μ_1 is the shear modulus of the elastic matrix, while μ_2 denotes the viscous coefficient of a Newtonian fluid. Table 3 depicts formulae for complex moduli $Q^*(z)/\mu_1$ and complex compliances $\mu_1/Q^*(z)$, $z = (I\omega\mu_2/\mu_1) - 1$ of the hexagonal array of fluid cylinders. Figures 3 and 4 present complex modulus $Q^*(z)/\mu_1$ and the real and imaginary parts of it, respectively.

Note that the modulus $Q^*(z)/(\mu_1)$ and compliance $\mu_1/Q^*(z)$, $z = (I\omega/\kappa) - 1$, $\kappa = \mu_1/\mu_2$ divided by $I\omega$ are the Fourier transforms of the torsional creep function $\Phi(t)$ and torsional relaxation function $\Psi(t)$, respectively, cf. [6]. Hence we can write

$$(7.2) \quad \mu_1 \overline{\Phi(I\omega)} = \frac{\mu_1}{I\omega Q^*(z)}, \quad \overline{\Psi(I\omega)} = \frac{Q^*(z)}{I\omega \mu_1}, \quad z = \frac{I\omega \mu_2}{\mu_1} - 1.$$

The inverse of the Fourier transformations of $\overline{\Phi(I\omega)}$ and $\overline{\Psi(I\omega)}$ take the forms, cf. Table 3 and Eq. (7.2)

$$(7.3) \quad \begin{aligned} \mu_1 \Phi(t) &= d^c + \sum_{n=1}^3 \frac{b_n^c}{a_n^c} \left(1 - (1 + a_n^c \kappa t) e^{-\kappa t} \right), \\ \frac{\Psi(t)}{\mu_1} &= d^r - \sum_{n=1}^3 \frac{b_n^r}{a_n^r} \left(1 - (1 + a_n^r \kappa t) e^{-\kappa t} \right). \end{aligned}$$

Here the coefficients d^c , d^r , b_n^c , b_n^r , a_n^c and a_n^r take values listed in Tables 4 and 5.

Table 3. The torsional moduli $Q(z)/\mu_1$ and $Q^{-1}(z)\mu_1$ for the inhomogeneous beam filled with the viscous fluid distributed in hexagonal array of cylinders: $Q(z)/\mu_1 = 1 + [3/3](z)$, $z = 1 - (I\omega/\kappa)$, $\kappa = \mu_1/\mu_2$; φ - the volume fraction.

φ	$\frac{Q^*(z)}{\mu_1}, z = \frac{I\omega}{\kappa} - 1, \kappa = \frac{\mu_1}{\mu_2}$	$\frac{\mu_1}{Q^*(z)}, z = 1 - \frac{I\omega}{\kappa}, \kappa = \frac{\mu_1}{\mu_2}$
0.76	$7.760 - \frac{60.980\kappa}{10.09\kappa - I\omega} - \frac{0.0974\kappa}{4.157\kappa - I\omega} - \frac{0.0431\kappa}{2.831\kappa - I\omega}$	$0.129 + \frac{0.0146\kappa}{4.196\kappa - I\omega} + \frac{0.0655\kappa}{2.887\kappa - I\omega} + \frac{0.9348\kappa}{2.124\kappa - I\omega}$
0.80	$9.957 - \frac{102.62\kappa}{12.56\kappa - I\omega} - \frac{0.1831\kappa}{3.814\kappa - I\omega} - \frac{.0218\kappa}{2.603\kappa - I\omega}$	$0.100 + \frac{0.0476\kappa}{3.911\kappa - I\omega} + \frac{0.0666\kappa}{2.643\kappa - I\omega} + \frac{0.9226\kappa}{2.095\kappa - I\omega}$
0.84	$14.01 - \frac{209.39\kappa}{17.27\kappa - I\omega} - \frac{0.4192\kappa}{4.210\kappa - I\omega} - \frac{0.0192\kappa}{2.477\kappa - I\omega}$	$0.071 + \frac{0.07551\kappa}{4.397\kappa - I\omega} + \frac{0.0925\kappa}{2.521\kappa - I\omega} + \frac{0.9011\kappa}{2.066\kappa - I\omega}$
0.88	$25.45 - \frac{737.96\kappa}{31.67\kappa - I\omega} - \frac{1.6569\kappa}{5.446\kappa - I\omega} - \frac{.02234\kappa}{2.388\kappa - I\omega}$	$0.039 + \frac{0.1339\kappa}{5.956\kappa - I\omega} + \frac{0.1471\kappa}{2.450\kappa - I\omega} + \frac{0.8608\kappa}{2.034\kappa - I\omega}$

Table 4.

φ	d^c	b_1^c	b_2^c	b_3^c	a_1^c	a_2^c	a_3^c
0.76	0.1289	0.0146	0.0655	0.9348	2.1958	0.8867	0.1238
0.80	0.1004	0.0476	0.0666	0.9226	1.9109	0.6432	0.0948
0.84	0.0714	0.0755	0.0925	0.9011	2.3972	0.5213	0.0656
0.88	0.0393	0.1339	0.1471	0.8608	3.9565	0.4500	0.0344

Table 5.

φ	d^r	b_1^r	b_2^r	b_3^r	a_1^r	a_2^r	a_3^r
0.76	7.7600	60.980	0.0974	0.0431	8.0939	2.1575	0.8312
0.80	9.9586	102.62	0.1831	0.0218	10.557	1.8143	0.6035
0.84	14.009	209.39	0.4192	0.0192	15.275	2.2101	0.4768
0.88	25.451	737.96	1.6569	0.0223	29.669	3.4456	0.3877

The torsional creep function $\Phi(t)$ and torsional relaxation function $\Psi(t)$ given by relations (7.3) and the values listed in Tables 4, 5 are depicted in Fig. 5.

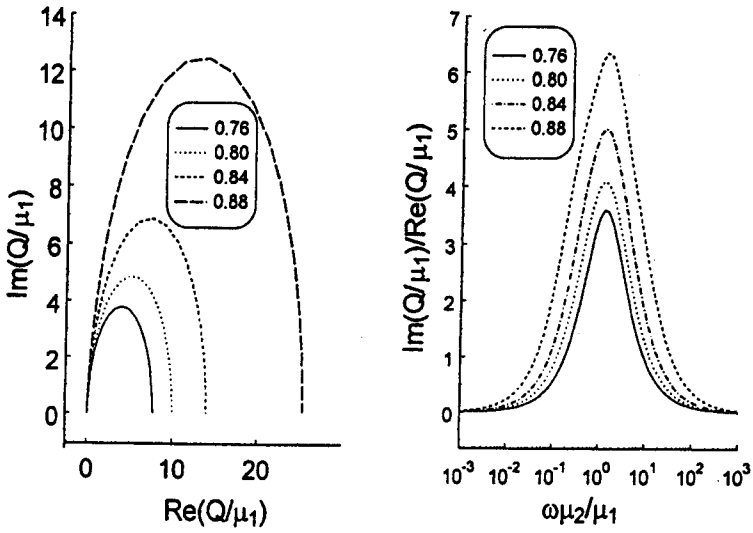


FIG. 3. Complex torsional modulus for the elastic beam filled with viscous fluid; $\varphi = 0.76, 0.80, 0.84, 0.88$.

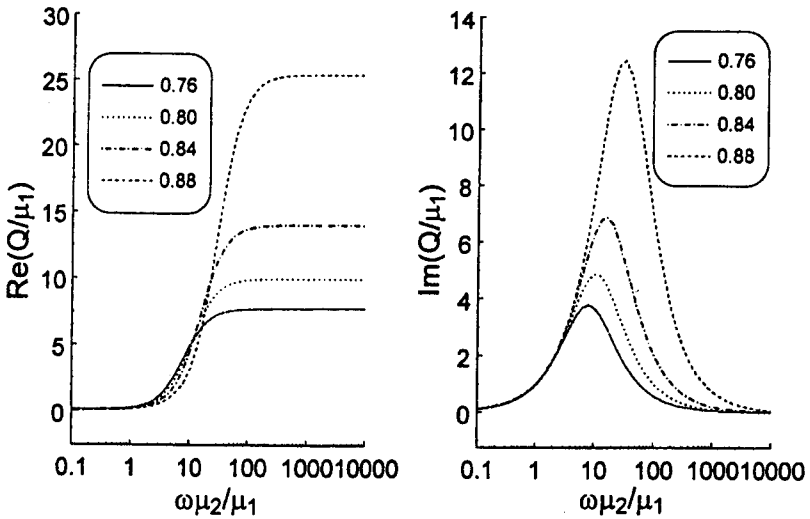


FIG. 4. Real and imaginary parts of the effective torsional modulus for the elastic beam filled with viscous fluid, $\varphi = 0.76, 0.80, 0.84, 0.88$.

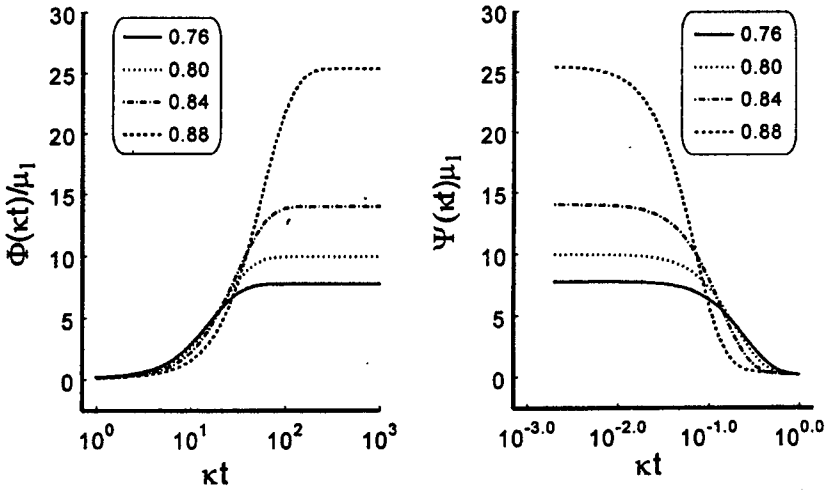


FIG. 5. The torsional creep function $\Phi(t)$ and torsional relaxation function $\Psi(t)$ for a porous beam consisting of hexagonal array of viscous fluid cylinders spaced in a linear elastic matrix.

8. TORSIONAL RIGIDITY OF PRISM-LIKE CANCELLOUS BONE

Most bones in the body have the dense compact bone forming an outer shell surrounding a core of spongy cancellous bone immersed in marrow, see Fig. 1b. In previous sections the macroscopic torsional modulus, torsional creep function and torsional relaxation function have been evaluated, cf. Tables 3 – 5 and Eq. (7.3).

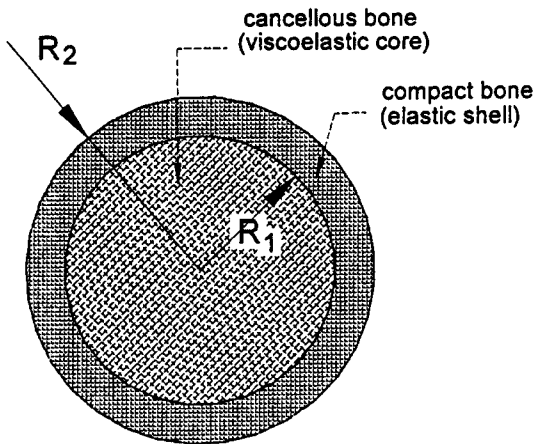


FIG. 6. An idealized model of typical human bone after the homogenization of cancellous bone process.

Consider now a homogeneous viscoelastic material surrounded by an elastic one. Such a composite models a prism-like human bone, see Fig. 6.

Two equivalent relationships between the torsional angle α and torsional moment M are commonly used for the torsional problem:

$$(8.1) \quad \overline{M(I\omega)} = I\omega \overline{\Psi^{ap}(I\omega)} \overline{\alpha(I\omega)} \quad \text{or} \quad \overline{\alpha(I\omega)} = I\omega \overline{\Phi^{ap}(I\omega)} \overline{M(I\omega)},$$

where

$$(8.2) \quad \frac{I\omega \overline{\Psi^{ap}(I\omega)}}{\mu_1} = \left(\iint_{S_j} dx dy + \frac{I\omega \overline{\Psi(I\omega)}}{\mu_1} \iint_{S_2} dx dy \right) \cdot \left(x^2 + y^2 + y \frac{\partial \overline{\beta(I\omega)}}{\partial x} - x \frac{\partial \overline{\beta(I\omega)}}{\partial y} \right).$$

Here $I\omega \overline{\Psi(I\omega)}$ and $I\omega \overline{\Phi(I\omega)}$ denote the torsional rigidity and torsional compliance of an inhomogeneous beam, respectively. The parameter μ_0 is the elastic modulus of the surrounding shell while $I\omega \overline{\Psi(I\omega)}$ denotes the effective shear modulus of the viscoelastic core, cf. Fig. 8. For a circular cross-section (see Fig. 8) we have $\beta(x, y, t) = 0$, thus $\beta(I\omega) = 0$. Formulae (8.1), (8.2) take the form

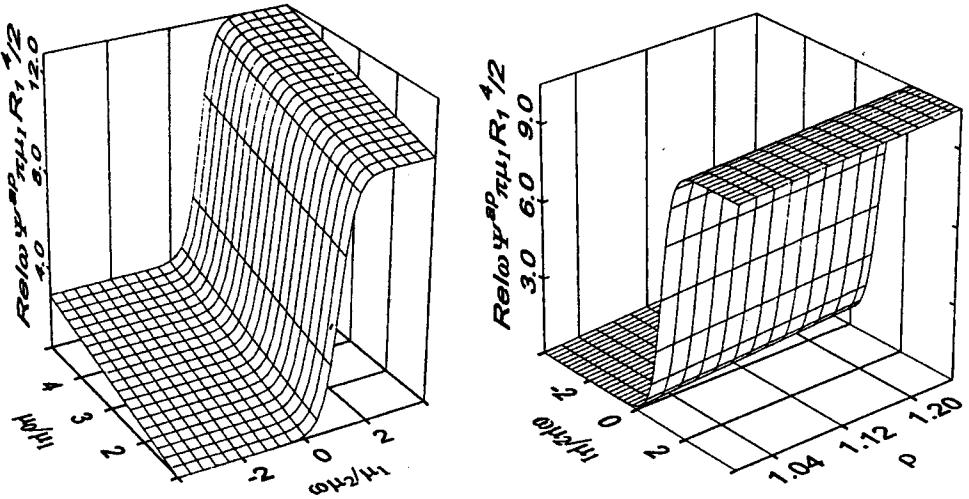


FIG. 7. Three-dimensional graphs of the torsional complex rigidities of bone showing the hydraulic stiffening due to the presence of marrow versus μ_0/μ_1 , $\omega\mu_2/\mu_1$ and ρ , $\omega\mu_2/\mu_1$.

$$(8.3) \quad \frac{2I\omega\overline{\Psi^{ap}}(I\omega)}{\pi\mu_1R_1^4} = \frac{\mu_0}{\mu_1}(\rho^2 - 1) + \frac{I\omega\overline{\Psi^{ap}}(I\omega)}{\mu_1}, \quad \rho = \frac{R_2^2}{R_1^2} \geq 1,$$

$$\frac{\pi R_1^4\mu_1 I\omega\overline{\Phi^{ap}}(I\omega)}{2} = \frac{1}{\left(\frac{\mu_1}{\mu_0}\right)^{-1}(\rho^2 - 1) + \frac{I\omega\overline{\Psi^{ap}}(I\omega)}{\mu_1}}, \quad \rho = \frac{R_2^2}{R_1^2} \geq 1.$$

The influence of the parameter ρ and ratios μ_0/μ_1 , $\omega\mu_2/\mu_1$ on the nondimensional torsional rigidity $2I\omega\overline{\Psi^{ap}}(I\omega)/\pi\mu_1R_1^4$ and nondimensional torsional compliance $\pi R_1^4\mu_1 I\omega\overline{\Phi^{ap}}(I\omega)$ have been investigated. The results are depicted in Figs. 7 and 8.

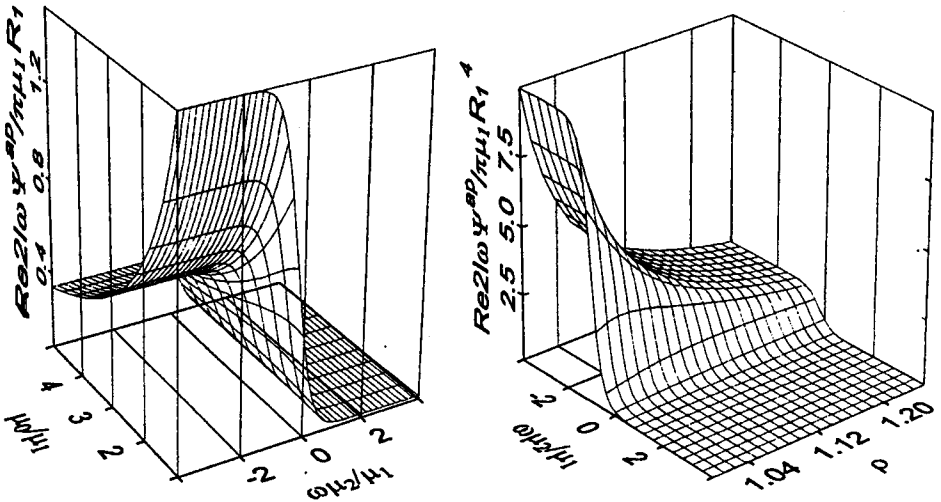


FIG. 8. Three-dimensional graphs of torsional complex compliances of bone showing a hydraulic stiffening due to the presence of marrow versus μ_0/μ_1 , $\omega\mu_2/\mu_1$ and ρ , $\omega\mu_2/\mu_1$.

9. FINAL REMARKS

In this study we have developed an idealized model of prism-like compact-cancellous bone structure. The cancellous bone is filled with marrow modelled as a viscoelastic fluid. The model predicts the mechanical response of prism-like cancellous structure loaded by torsional moments. The analytical formulae relating the torsional rigidity, compliance, creep function and relaxation function with apparent density, viscosity of marrow and elastic parameters have been obtained. Those formulae predict the hydraulic stiffening of a human bone due

the presence of bone marrow. The next step will consist in the elaboration of a three-dimensional model. A challenging problem is to investigate the aging effects of bone and marrow.

ACKNOWLEDGMENT

The authors were supported by the State Committee for Scientific Research (KBN Poland) through the grant No 8 T11F 017 18. The first author was also supported by the grant No 7 T07A 021 15.

REFERENCES

1. G. A. BAKER, *Best error bounds for Padé approximants to convergent series of Stieltjes*, J. Math. Phys., **10**, 814–820, 1969.
2. G. A. BAKER, P. GRAVES-MORRIS, *Padé Approximants*, Second Edition, GIAN-CARLO ROTA, [Eds.], [In:] *Encyclopedia of Mathematics and its Applications*, **59**, Cambridge University Press, Cambridge 1996.
3. G. S. BEAUPRÈ, W. C. HAYES, *Finite element analysis of a three dimensional opened-celled model for trabecular bone*, J. Biomech. Engng., **107**, 249–256, 1985.
4. A. BENSOUSSAN, J. L. LIONS, G. PAPANICOLAOU, *Asymptotic analysis for periodic structures*, North-Holland, Amsterdam 1978.
5. D. R. CARTER, W. C. HAYES, *The compressive behaviour of bone as a two-phase porous structure*, J. Bone Jt. Surg., **59A**, 954–962, 1977.
6. R. M. CHRISTENSEN, *Mechanics of composite materials*, John Wiley&Sons, New York 1979.
7. D. CIORANESCU, J. SAINT JEAN PAULIN, *Homogenization of reticulated structures*, Springer-Verlag, New York 1999.
8. D. CIORANESCU, J. SAINT JEAN PAULIN, *Asymptotic analysis of elastic wireworks*, Laboratoire d'analyse numerique, R89008, Université Paris 1989.
9. N. L. FAZZALARI, J. DARRACOTT, B. VERNON-ROBERTS, *Histomorphometric changes in the trabecular structure of a selected stress region in the femur in patients with osteoarthritis and fracture of the femoral neck*, Bone, **6**, 125–133, 1985.
10. J. L. GIBSON, *The mechanical behaviour of cancellous bone*, J. Biomechanics, **18**, 317–328, 1985.
11. L. J. GIBSON, M. F. ASHBY, *Cellular solids: structure and properties*, Pergamon Press, New York 1988.
12. K. GOLDEN and G. PAPANICOLAOU, *Bounds for effective parameters of heterogeneous media by analytic continuation*, Comm. Math. Phys., **90**, 473–491, 1983.
13. X. E. GUO, T. A. MCMAHON, T. M. KEAVENY, W. C. HAYES, L. GIBSON, *Finite modelling damage accumulation in trabecular bone under cycling loading*, J. Biomechanics, **27**, 145–155, 1994.

14. T. P. HARRIGAN, M. JASNY, R. W. MANN, W. H. HARRIS, *Limitation of the continuum assumption in cancellous bone*, J. Biomechanics, **21**, 269–275, 1988.
15. S. J. HOLLISTER, D. P. FYHIRE, K. J. JEPSEN, S. A. GOLDSTEIN, *Application of homogenization theory to the study of trabecular bone mechanics*, J. Biomechanics, **24**, 825–839, 1991.
16. M. KASRA, M. D. GRYPAS, *Static and dynamic finite element analyses of an idealized structural model of vertebral trabecular bone*, J. Biomech. Engng., **120**, 267–272, 1998.
17. R. B. MARTIN, D. B. BURR, N. A. SHARKEY, *Skeletal Tissue Mechanics*, Springer-Verlag, New York 1998.
18. J. MCELHANEY, N. ALEM, V. ROBERTS, *A porous block model for cancellous bones*, ASME Publication No 70-WA/BHF-2, 1–9, 1970.
19. N. I. MUSHELISHVILI, *Some basic problems of mathematical theory of elasticity* [in Russian], Nauka, Moskva 1966.
20. R. MÜLLER, P. RÜEGSEGGER, *Micro-tomographic imaging for the nondestructive evaluation of trabecular bone architecture*, [In:] *Bone Research in Biomechanics*, G. LOWET, P. RÜEGSEGGER, H. WEINANS and A. MEUNIER [Eds.], 61–79, IOS Press, Amsterdam 1997.
21. J. A. OCHOA, D. A. HECK, K. D. BRANDT, B. M. HILLBERRY, *The effect of intertrabecular fluid on femoral head mechanics*, J. of Reumatology, **18**, 580–584, 1991.
22. J. SAINT, J. PAULIN, *Développement asymptotique et calcul de correcteurs pour la torsion élastique d'arbres à cavités cylindriques*, Report No 78021, Analyse Numérique Université Pierre et Marie Curie, 1978.
23. W. T. PERRINS, D. R. MCKENZIE, R. C. MC PHEDRAN, *Transport properties of regular array of cylinders*, Proc. R. Soc. Lond., **A 369**, 207–225, 1979.
24. J. W. PUGH, R. M. ROSE, E. L. RADIN, *A structural model for the mechanical behavior of trabecular bone*, J. Biomechanics, **6**, 657–670, 1973.
25. E. SANCHEZ-PALENCIA, *Non-homogeneous media and vibration theory*, Springer, Berlin 1980.
26. M. TAVASSOLI, J. M. YOFFEY, *Bone marrow: structure and function*, Alan R. Liss, New York 1983.
27. J. TELEGA, A. GAŁKA, S. TOKARZEWSKI, *Effective moduli of trabecular bone*, Acta Bioeng. Biomech., **1**, 53–57, 1999.
28. J. J. TELEGA, A. GAŁKA, S. TOKARZEWSKI, *Application of the reiterated homogenization to determination of effective moduli of a compact bone*, J. Theor. Appl. Mech., **37**, 687–706, 1999.
29. J. J. TELEGA, T. LEKSZYCKI, *Progress in functional adaptation of tissues and remodelling*, Part I. Bone structure, its properties and models, Engng. Trans., (in preparation).
30. S. TOKARZEWSKI, *N-point Padé approximants to real-valued Stieltjes series with nonzero radii of convergence*, J. Comp. Appl. Math., **75**, 259–280, 1996.
31. S. TOKARZEWSKI and J. J. TELEGA, *S-continued fraction method for the investigation of a complex dielectric constant of two-phase composite*, Acta Appl. Math., **49**, 55–83, 1997.
32. S. TOKARZEWSKI, J. J. TELEGA, *Bounds on effective moduli by analytical continuation of the Stieltjes function expanded at zero and infinity*, Z. angew. Math. Phys., **48**, 1–20, 1997.
33. S. TOKARZEWSKI, J. J. TELEGA, A. GAŁKA, *A contribution to evaluation of effective moduli of trabecular bone with rod-like microstructure*, J. Theor. Appl. Mech., **37**, 3, 707–728, 1999.

34. R. S. WEINSTEIN, M. S. HUTSON, *Decreased trabecular width and increased trabecular spacing contribute to loss with aging*, *Bone*, **8**, 137-142, 1987.
35. J. L. WILLIAMS, J. L. LEWIS, *Properties and anisotropic model of cancellous bone from the proximal tibia epiphysis*, *J. Biomech. Engng.*, **104**, 50-56, 1982.

Received November 10, 2000.
